J Oceanogr (2011) 67:699–708
DOI 10.1007/s10872-011-0080-x

SPECIAL SECTION: ORIGINAL ARTICLE

Regional Environmental Oceanography in the South China Sea and Its Adjacent Areas (REO-SCS): II

Characteristics and mechanisms of the upwelling in the southern Taiwan Strait: a three-dimensional numerical model study

Yuwu Jiang · Fei Chai · Zhenwen Wan · Xin Zhang · Huasheng Hong

Received: 18 August 2010 / Revised: 9 September 2011 / Accepted: 24 September 2011 / Published online: 28 October 2011

Abstract Using a nested circulation model based on the Princeton Ocean Model, we investigate the characteristics and mechanisms of two main upwellings in the southern Taiwan Strait: the Southwest upwelling and the Taiwan Bank upwelling. The Southwest upwelling exists in summer when the southwesterly monsoon dominates, and the Taiwan Bank upwelling occurs over a longer period from May to September. The upslope current over a distinctly widened shelf transports the cold water on-shoreward at the lower layer and the southwesterly monsoon wind drives the cold water to the surface layer, forming the Southwest upwelling, while tidal residual current weakens the upslope advection. For the Taiwan Bank upwelling, the upward transport of the South China Sea water due to the Bank topography carries the cold water from the subsurface layer to the depth of approximately 25 m near the Taiwan Bank, then the strong tidal mixing forces this upwelled water further upward to the surface layer.

Keywords Upwelling · Numerical model · Tidal processes · Taiwan Strait

Y. Jiang (✉) · Z. Wan · H. Hong
State Key Laboratory of Marine Environmental Science, Xiamen University, Fujian 361005, China
e-mail: ywjiang@xmu.edu.cn

F. Chai
School of Marine Sciences, University of Maine, Orono, ME 04469, USA

X. Zhang
Institute of Remote Sensing Applications, Chinese Academy of Sciences, Beijing 100101, China

1 Introduction

Coastal upwelling is an important marine system which can transport nutrient-rich water towards the ocean surface. The mechanisms of the coastal upwelling are associated with the wind stress, topography and tidal processes, etc. Most of the coastal upwellings, e.g., the Canary upwelling, the Benguela upwelling, the California upwelling and the Peru upwelling, are caused by the Ekman transport driven by the equator-ward trade wind stress plus Coriolis effect. The topography effect was studied by Arthur (1965) who demonstrated that the vorticity will change along the streamline when the boundary flows pass a cape, and the upwelling will be generated at the lee of the cape. As it comes to the bottom topography, the downstream variations of the bathymetry will change the vorticity and therefore induce the vertical velocity under the nonlinear effect at first order (e.g., Blanton et al. 1981; Janowitz and Pietrafesa 1982), meanwhile the wind-driven upwelling can be enhanced by the interaction of the bottom friction with the topography (e.g., Pringle 2002). The upwelling may relate with the tidal processes through many ways. For example, the tide-induced cross-shore residual current accounts for the cold water at the lower part of the upwelling region, and the strong tidal vertical mixing can transport these waters to the surface near south-west Nova Scotia (Tee et al. 1993); the upwelling can be caused by the centrifugal forces when strong tidal currents flow along the convex peninsula coastline (Garret and Loucks 1976). The second cross-shore circulation associated with the tidal processes will generate the upwelling at Georges Bank (e.g., Loder and Wright 1985).

Connecting the South China Sea (SCS) with the East China Sea (ECS), the Taiwan Strait (TWS) is located in the Northwest Pacific (Fig. 1). As a part of the continental

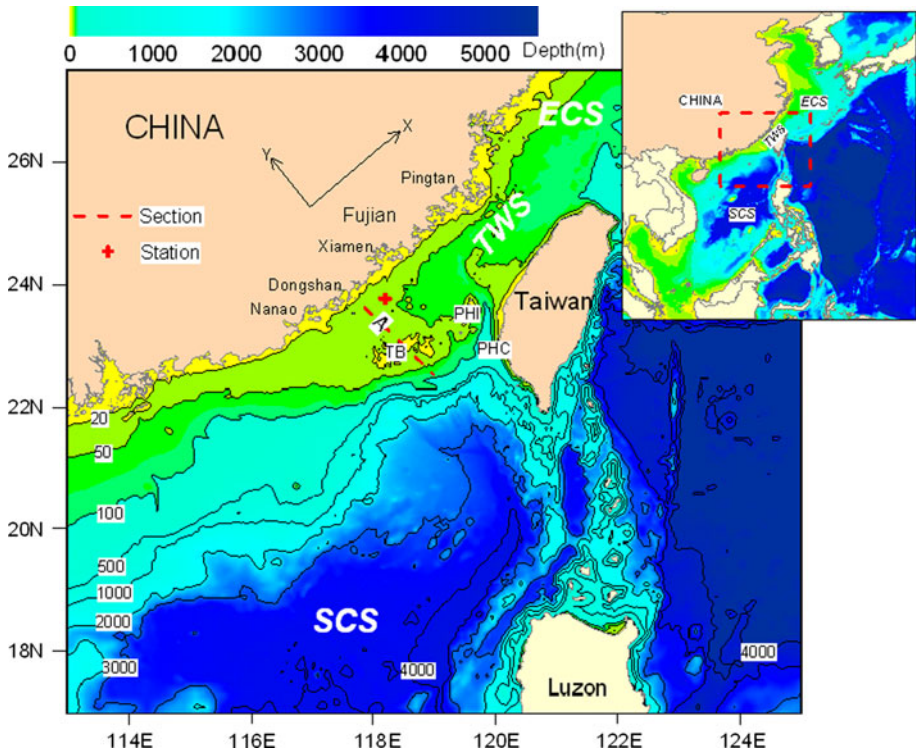

Fig. 1 Bathymetry and model domain (*left* sub-domain, *upper-right* all-domain). + is the station where the surface velocity is observed by the high frequency radar and *dashed line* is the cruise Section A. The coordinate system is oriented so that x is along-shore and y is cross-shore. *SCS*, *ECS*, *TWS*, *TB*, *PHC* and *PHI* denote the South China Sea, the East China Sea, the Taiwan Strait, the Taiwan Bank, the Penghu Channel and the Penghu Island, respectively

shelf, the complex seafloor topography of the southern TWS varies from a depth of 30 m in the west to 70 m in the east, with a maximum depth deeper than 1,000 m to the southeast. The Taiwan Bank is the shallowest, at approximately 20 m depth. The Penghu Channel, located between the Penghu Island and the Taiwan Island, forms the main way for the southern warm current flowing into the TWS (Jan et al. 2006). Alternating strong northeasterly monsoons in winter (from October to April) and weak southwesterly monsoons in summer (from June to August) influence the TWS (Hellerman and Rosenstein 1983; Jan et al. 2002). In summer, the SCS Warm Current flows northeastward along the continental shelf break and extends to the TWS (Guan and Chen 1964; Hu et al. 2010).There are two upwelling regions in the southern TWS in summer: the upwelling near Dongshan in the southwestern TWS (hereafter, the Southwest upwelling), and the upwelling around the Taiwan Bank (Taiwan Bank upwelling) (Hong et al. 1991; Hu et al. 2003; Tang et al. 2002).

Most of the previous works have pointed out that the favorable southwesterly monsoon is the mechanism of Southwest upwelling (e.g., Guan and Chen 1964; Cai and Lennon 1988; Lin et al. 1999), while others proposed that the ascending bottom current may be the mechanism (Li and Li 1989; Hu and Liu 1992). Recently, Gan et al. (2009) showed that the widened shelf can induce the cross-shore transport of the cold water under the favorable wind, and Jing et al. (2011) found that offshore Ekman drift in the summer of 1998 was the strongest over the past 18 years, and it was the major dynamic factor to induce the abnormally strong upwelling during 1998. As for the Taiwan Bank upwelling, Cai and Lennon (1988) described how the combination of Kuroshio intrusion and the topography is the mechanism. Wu and Lin (1990) indicated that ascending bottom current and monsoon are important factors. Qiao et al. (2008) found that the upwelling will disappear at the surface without the tidal process, and mentioned further work was needed to discover the mechanism of the Taiwan Bank upwelling.

Therefore, the cross-shore current, favorable wind and tide may be the mechanism of the Southwest upwelling and the Taiwan Bank upwelling. How they function on these two upwellings and which role they play are the purposes of this study. Using a high-resolution nested circulation model based on the Princeton Ocean Model (POM) (Mellor 2004), we investigate these two upwellings. Sections 2 and 3 describe the model configuration and performance, and Sect. 4 discusses the characteristics and mechanisms of the two upwellings, including the role of tidal processes in affecting upwelling. Finally, Sect. 5 presents a summary.

2 Model configuration

This study uses a POM-based model to simulate the key physical processes in the TWS. The entire model domain (all-domain) covers the Northwest Pacific with a coarse

resolution of 0.2°, and the sub-domain covers the TWS area with a high spatial resolution of 0.04° (Fig. 1). Vertically, both all-domain and sub-domain have 21 sigma levels, and two values, KL1 and KL2, in sigma coordinates are 6 and 19, respectively, suggesting a higher resolution near the surface. The model bathymetry is a spatially filtered version combining the survey data and ETOPO2v2 from the National Geophysical Data Center. The filter has made the local slope factor, $\delta h/h$ (h is water depth), smaller than 0.3 so as to reduce the unexpected diapycnal mixing caused by sigma coordinates (Mellor et al. 1998; Mellor 2004).

The nested method used in this study was similar to the one developed by Oey and Chen (1992) except one-way nesting was used here for long-term running. At first, a relaxation zone of 0.5° width was defined at the sub-domain boundary, and a one-way nesting was maintained by sending information, i.e. surface elevation, temperature and salinity, from the outer all-domain to the relaxation zone of the sub-domain. The topography in the relaxation zone of the sub-domain is interpolated from the all-domain, and the topography of the all-domain in the overlapping area is the averaged value of the related grids in the sub-domain. The different strategies proposed by Oey and Chen (1992) were also adopted for the inflow and outflow conditions in the relaxation zone to avoid altering signals translating from all-domain to sub-domain. In this study, the external time steps were 30 and 5 s for the all-domain and sub-domain, respectively, and both domains used the same internal time step, 300 s.

For the all-domain, the temperature, salinity, surface elevation and velocity, derived from a Pacific Regional Ocean Model System (Pacific ROMS) (Wang and Chao 2004; Liu and Chai 2009), were set as the lateral boundary and initial conditions. In addition, at the open boundary of the sub-domain, this model includes tidal forcing comprising 16 tidal components (M_2, S_2, K_1, O_1, N_2, P_1, K_2, Q_1, M_1, J_1, OO_1, $2N_2$, Mu_2, Nu_2, L_2 and T_2) available from the tidal dataset Nao.99b (version 2000.09.09) (Matsumoto et al. 2000). Additionally, the monthly river discharges along the China coast were included in the model as freshwater sources from the major rivers, e.g., the Yangtze, the Pearl, the Minjiang, and the Jiulongjiang Rivers. The tide-generating forcing is not included in the model. For the air–sea interface, the net heat and net freshwater fluxes at the air–sea interface were provided by the data from the Mercator Ocean (http://www.mercator-ocean.fr), and the wind stress was derived from daily averaged data of QuikSCAT at 0.25° resolution. With the use of data from 2 buoys in the TWS, Chen (2011) estimated the root-mean-square-errors (RMSEs) of the magnitude and direction of the wind from QuikSCAT to be 1.1 m s^{-1} and 22.83°, respectively.

3 Model evaluation

To evaluate the model performance on reproducing the characteristics and processes of the upwellings in the southern TWS, the model ran from July 1999 to November 2009, when the QuikSCAT data was available. The following comparisons indicate acceptable agreements between the model results and the observed data.

3.1 Tidal harmonic constant

After the model ran for 4 years, the following 1-month time series of hourly water elevation in the sub-domain was analyzed to obtain the tidal harmonic constants, i.e. M_2, S_2, K_1 and O_1. Figure 2 shows a comparison of the modeled M_2 tidal patterns with the observed data at gauge stations. It is indicated that the RMSEs for total 45 stations are 0.093 m in amplitude and 6.5° in phase. The maximum values are 0.23 m and 23°, respectively, near the tidal nodal band southwest of the Taiwan Island. The modeled M_2 patterns are consistent with the results of Fang et al. (1999). From Fig. 2, it is clear that the tidal waves propagate southwestward from the ECS and rebound at the continental slope in the southern TWS, resulting in a large tidal range in the western TWS, which agrees with the previous study by Jan et al. (2004).

3.2 Surface current

There was a high frequency (HF) radar system in the southwestern TWS (Jiang 2007). The 1-month surface current data (totally 3,322 observations) at station + (Fig. 1) in August 2008 were used in this study. The relationship between model and HF radar surface currents is plotted in Fig. 3. The correlation coefficient and RMSE of along-shore velocity are 0.88 and 0.17 m s^{-1}, respectively, and those of cross-shore velocity are 0.83 and 0.14 m s^{-1}, respectively. With the use of an inertial cycle (about 31 h) boxcar filter, we excluded the tidal and inertial components of the velocity. Figure 4 presents the comparison of low-pass filtered velocity in August 2008, and the correlation coefficient and RMSE of the along-shore filtered velocity are 0.81 and 0.08 m s^{-1}, respectively, and those of cross-shore filtered velocity are 0.65 and 0.08 m s^{-1}, respectively. Both the model and HF radar data show the along-shore velocity is northeastward at a mean value of about 0.2 m s^{-1}, and the cross-shore velocity is mostly off-shoreward at a maximum value of about 0.2 m s^{-1} (corresponding to Ekman drift at surface layer under the southwesterly monsoon), except for two periods around August 5 and 21 when two typhoons (named as Kammuri and Nuti) passed, inducing a maximum on-shore current of 0.2 m s^{-1}.

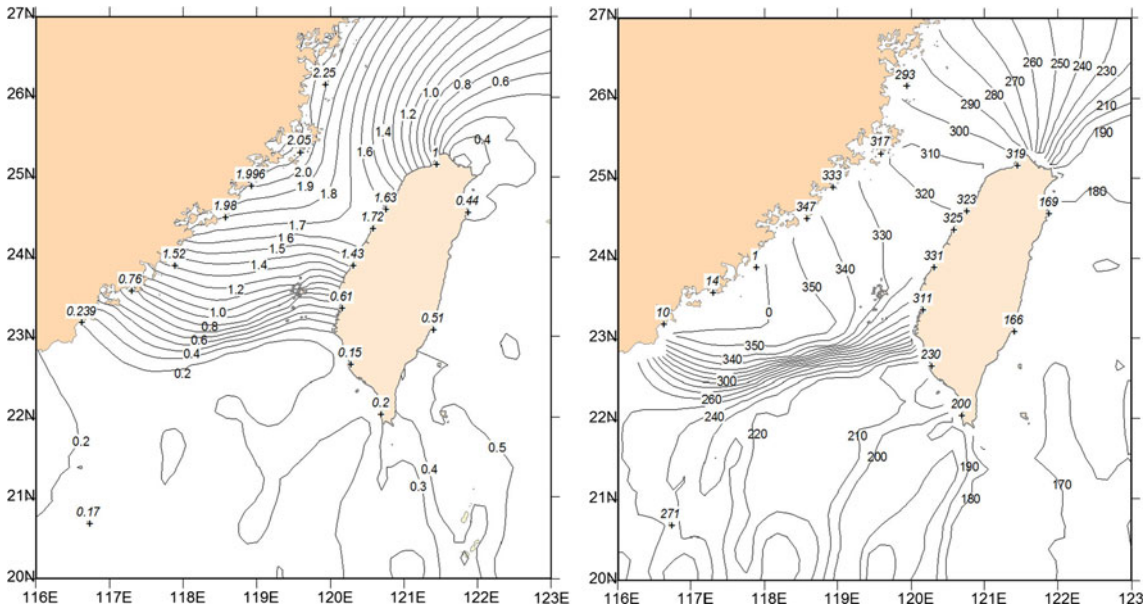

Fig. 2 Distribution of amplitude (*left*) and phase (*right*) of the M_2 tide (contours are the modeled result, and + shows the tidal gauge station with the observed value in *italics*)

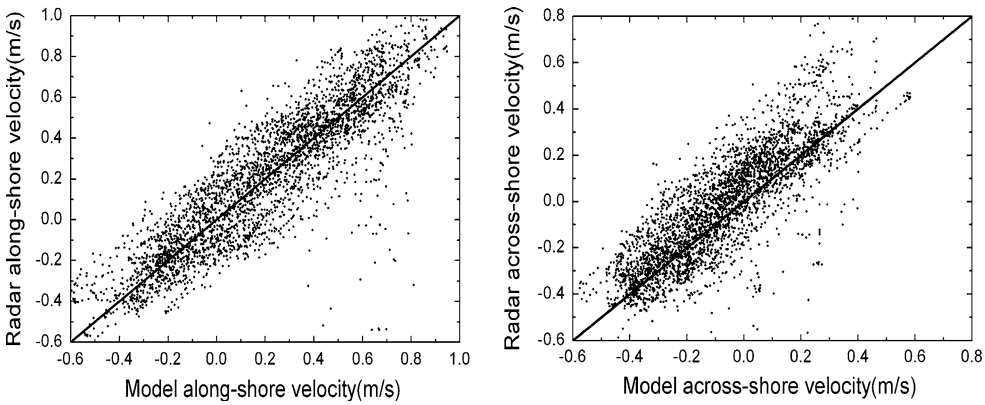

Fig. 3 Relationships between the model–HF radar surface velocity based on 3,322 samples in August 2008 at station + (see Fig. 1). The correlation coefficient and RMSE of along-shore velocity (*left*) are 0.88 and 0.17 m s^{-1}, respectively, and those of cross-shore velocity (*right*) are 0.83 and 0.14 m s^{-1}, respectively

3.3 Sea surface temperature (SST)

Daily MODIS (Moderate Resolution Imaging Spectroradiometer) Aqua Level-2 SST data were obtained from the US NASA Goddard Space Flight Center (GSFC) and then mapped to a cylindrical equidistant projection at 1 km/pixel resolution (Zhang et al. 2006). Figure 5a and b shows monthly averaged SST in July 2005, derived from the MODIS data and the model, respectively. It is evident that the SST pattern in the TWS was simulated well by depicting a high level of agreement in the two main upwelling regions, the Southwest upwelling and the Taiwan Bank upwelling (demonstrated by dashed ellipses E1 and E2 in Fig. 5b). Both the model result and the MODIS data indicate that the SST in the upwelling regions is lower than 26°C, and the lowest SST reaches 25°C in the center of the upwelling region.

3.4 Vertical hydrographic structure

The CTD data collected from the southern TWS cruise in July 2005 were used to further evaluate the model performance in terms of representing the vertical hydrographic structure in the upwelling regions. Figure 6a, b show that the observed and modeled temperature distributions at Section A (Fig. 1) across the Southwest upwelling and the Taiwan Bank upwelling. The modeled temperature distribution matches reasonably well with the observed one, with RMSE of 0.83°C between the observations and the model results. The model reproduces the upwelling cores well, indicating that the cold water of 24°C can extend 25 km offshore in the Southwest upwelling, and the water colder than 26°C appears at the surface in the Taiwan Bank upwelling.

4 Upwelling analysis

In order to investigate the dynamics and controlling factors of the Southwest upwelling and the Taiwan Bank upwelling, the climatological results in Fig. 7 are obtained though averaging parameters of hindcast calculation from July 2000 to November 2009.

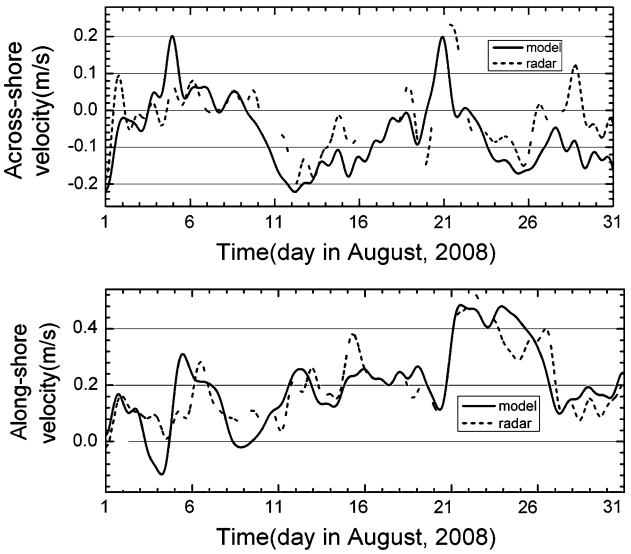

Fig. 4 The comparisons of low-pass filtered velocity from model and HF radar in August 2008 at station + (see Fig. 1). The correlation coefficient and RMSE of along-shore filtered velocity (*top*) are 0.81 and 0.08 m s^{-1}, respectively, and those of cross-shore filtered velocity (*bottom*) are 0.65 and 0.08 m s^{-1}, respectively

Figure 7a1, a2 show the time–depth variations of the area-averaged vertical velocity in two regions (ellipses E1 and E2 shown in Fig. 5b), where the upwelling frequently appears according to previous studies (Hu et al. 2003). The modeled vertical velocity shows a strong seasonal cycle of vertical motion near Dongshan (Fig. 7a1), but a steady and approximately year-round upwelling around the Taiwan Bank (Fig. 7a2). Figure 7b1, b2 present the temperature difference between the inside and along the ellipses in the two regions.

4.1 Characteristics and mechanism of the Southwest upwelling

As shown in Fig. 7a1, the modeled vertical velocity has a positive value in summer and reaches the maximum of about 4×10^{-5} m s^{-1} in mid-July, and the contour of 2×10^{-5} m s^{-1} arches upward to the upper layer. Figure 7b1 shows that the area-averaged temperature in the region (E1) is lower than that along the ellipse by 0.5°C in summer, and the maximum temperature difference reaches 1°C in July. The upwelling periods calculated from the present model are consistent with the observational data summarized in Hu et al. (2003).

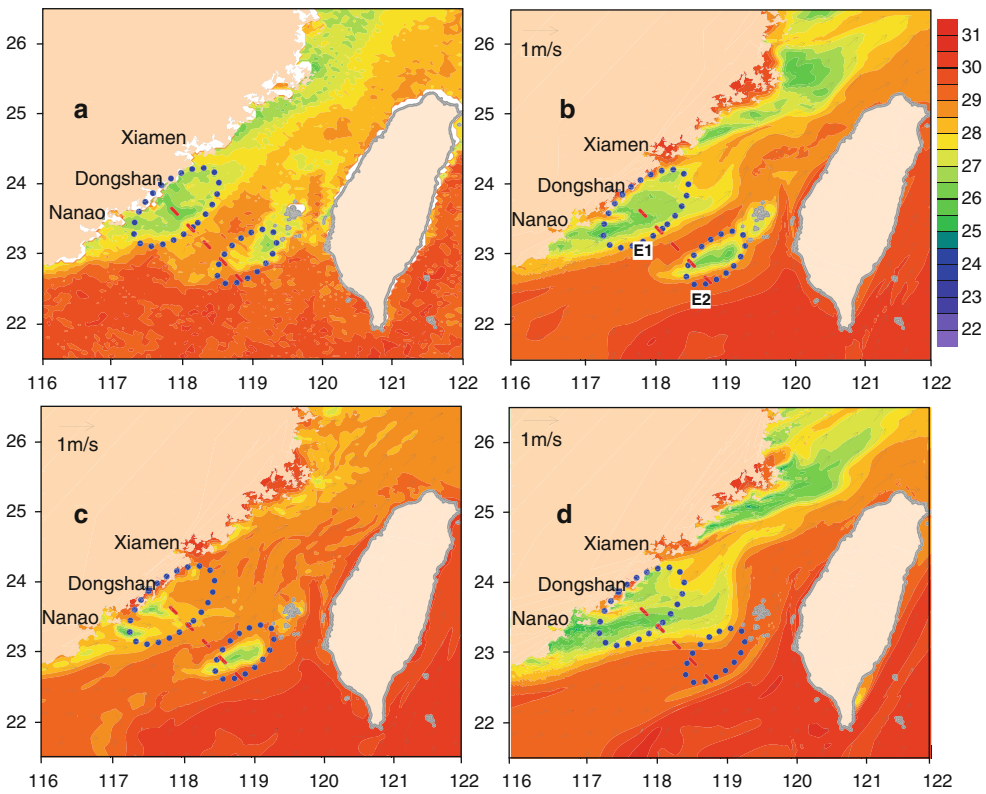

Fig. 5 SST distribution in July 2005. **a** SST from the MODIS data; and the modeled temperature and currents at the surface layer in the normal case (**b**), no wind case (**c**) and no tide case (**d**). Two areas with distinctly low temperature, i.e. the Southwest upwelling and the Taiwan Bank upwelling, are identified by *blue dashed ellipses* (*E1* and *E2*). The *red dashed line* is the location of Section A

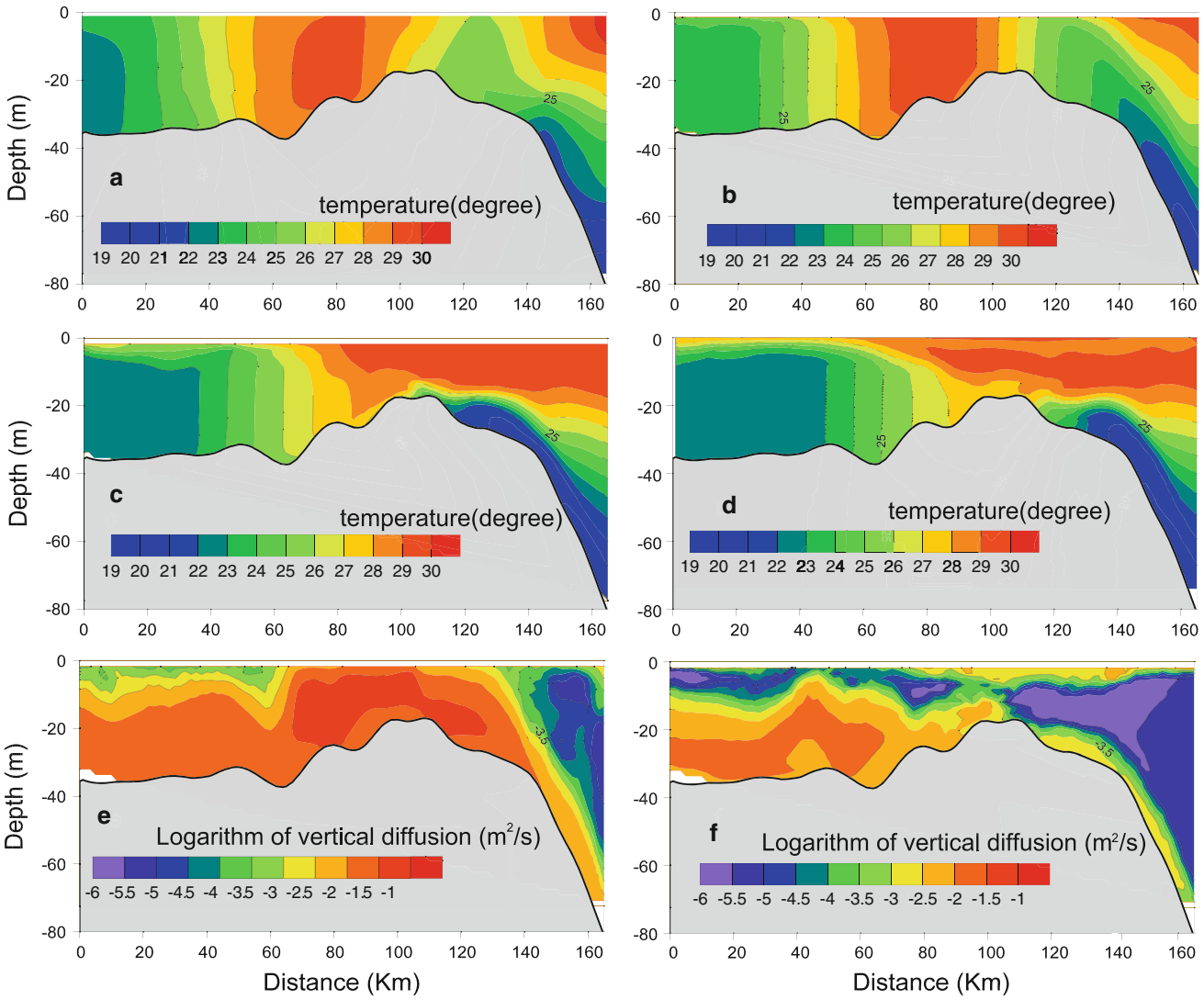

Fig. 6 Temperature distribution along Section A (see Fig. 1) from the observations (**a**), the model of the normal case (**b**), no tidal case (**c**) and no wind and no tide case (**d**); the vertical diffusion rate from the model of normal case (**e**) and no tide case (**f**) on July 10–11, 2005

The model sensitive tests were carried out to test the wind-driven mechanism of the Southwest upwelling. Driven by the normal winds (southwesterly in July 2005), the upwelling pattern (Fig. 5b) can be reproduced, which is similar to the MODIS data (Fig. 5a). In contrast, the wind was set to zero in the model sub-domain while the all-domain was still driven by the normal winds to maintain a circulation pattern similar to normal simulation. As the initial condition includes the effects of formerly local winds, the influence will last about 15 days. The following sensitivity results were achieved when the model had been run from initial condition for 15 days. Without local winds, the cold water still exists near Nanao and Dongshan, but reducing the area considerably (Fig. 5c). This result indicates that the favorable local wind is the main mechanism for the Southwest upwelling. Gan et al. (2009) examined the Southwest upwelling under a favorable wind and demonstrated that the shoreward transport is enhanced by a quasi-barotropic along-isobath pressure gradient and the converging isobaths at the head of the widened shelf (near 22°N, 116°E). This shoreward transport is advected downstream with the coastal current and outcrops on the lee side of the coastal cape near Nanao under the favorable wind. In the test without the local wind and tide, the cold water can still appear in the lower layer outside Dongshan without outcropping at the surface (Fig. 6d), which shows the shoreward transport of the cold water mentioned above is not associated with the wind and tide. It is also noted that the lower layer cold water from the head of the widened shelf (nearshore of Shanwei, southwest of Dongshan) can be transported to the lower layer near Dongshan, but it cannot be upwelled to the surface without the favorable wind-driven Ekman transport.

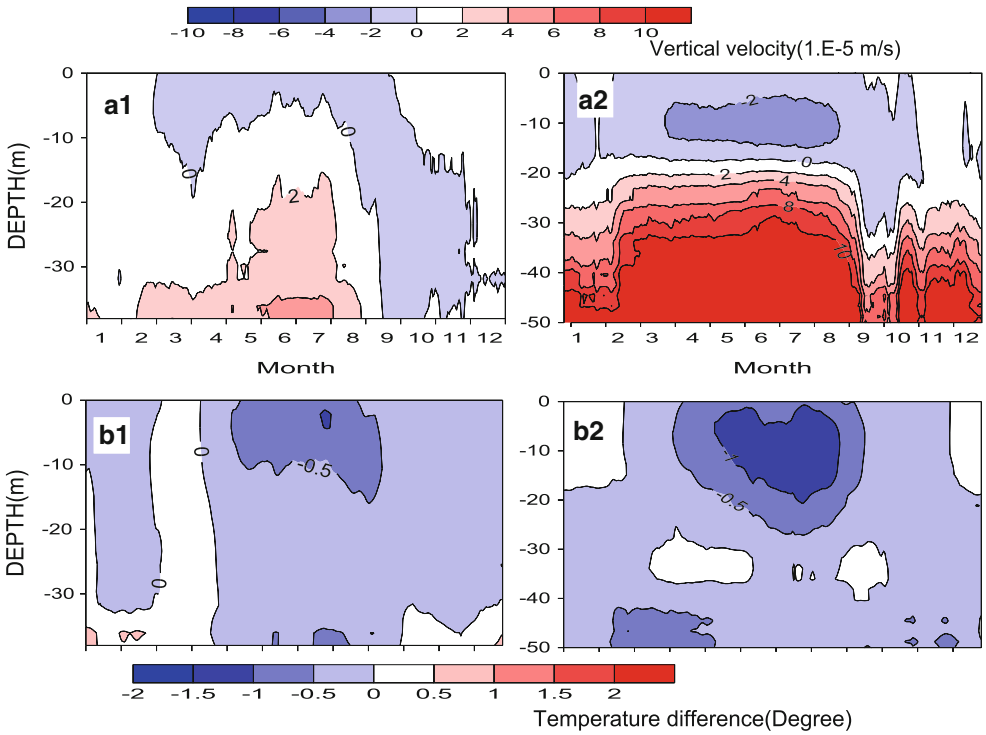

Fig. 7 Time–depth variations of the area-averaged vertical velocity (in 10^{-5} m s^{-1}) in the upwelling regions (referring to ellipses E1 and E2 in Fig. 5b), i.e. the Southwest upwelling (**a1**) and the Taiwan Bank upwelling (**a2**). Time–depth variations of the averaged temperature difference (in degree) between inside and along the ellipses, i.e. the Southwest upwelling (**b1**) and the Taiwan Bank upwelling (**b2**)

4.2 Characteristics and mechanism of the Taiwan Bank upwelling

Figure 7a2 shows a different vertical velocity structure near the southeast of the Taiwan Bank (E2 in Fig. 5b), with the positive values (upwelling) below 25 m (approximately 10×10^{-5} m s^{-1} at 35 m) throughout the year. The seasonal wind-driven Ekman transport cannot cause this year-round positive vertical velocity because the upwelling-favorable southwesterly monsoon only occurs from June to August. As mentioned previously, the SCS Warm Current flows northeastward along the shelf break on the southeast side of the Taiwan Bank almost year-round, as depicted in Fig. 5b in summer. The transport of SCS water due to the Taiwan Bank topography leads to a positive vertical velocity year-round on the slope southeast of the Taiwan Bank.

The Taiwan Bank is mostly shallower than 25 m, but the positive vertical velocity in the Taiwan Bank upwelling region (E2 in Fig. 5b) extends from 25 m down to the deep sea (Fig. 7a2), evidencing that the water ascends from the lower layer. However, the vertical velocity near the surface is negative and varies seasonally (Fig. 7a2), while the temperature difference between the inside and along the ellipse (E2 in Fig. 5b) exceeds 1°C in summer (Fig. 7b2). This raises an interesting question: how does the cold water upwell from 25 m to the surface without a positive vertical velocity?

4.3 The role of the tides in upwelling

Tide can modify the seasonal circulation and corresponding upwelling processes in the area with a large tidal range (Xue et al. 2000; Qiao et al. 2008). In the region characterized by tide-amplifying topography, such as the Georges Bank and the Taiwan Bank, the tide–topography interaction may generate cross-isobaths residual circulation and tidal mixing (Zimmerman 1978; Chen et al. 1995). For the stratified waters, internal tide may be induced over favorable bathymetry including the shelf break area, which can create internal turbulence and vertical mixing and also change water properties (Holloway and Barnes 1998; Garret 2003).

The southern TWS has been characterized as an area not only with strong tidal energy (Jan et al. 2004) but also having internal tides (Hsu et al. 2000), so the tidal processes may play a role in modifying the upwelling dynamics. In order to evaluate the effect of the strong tidal processes on the two upwelling regions in the southern TWS, sensitive tests were conducted with and without tides. The initial condition was set to the results modeled on July 2, 2005, and the cases with normal forcing (with

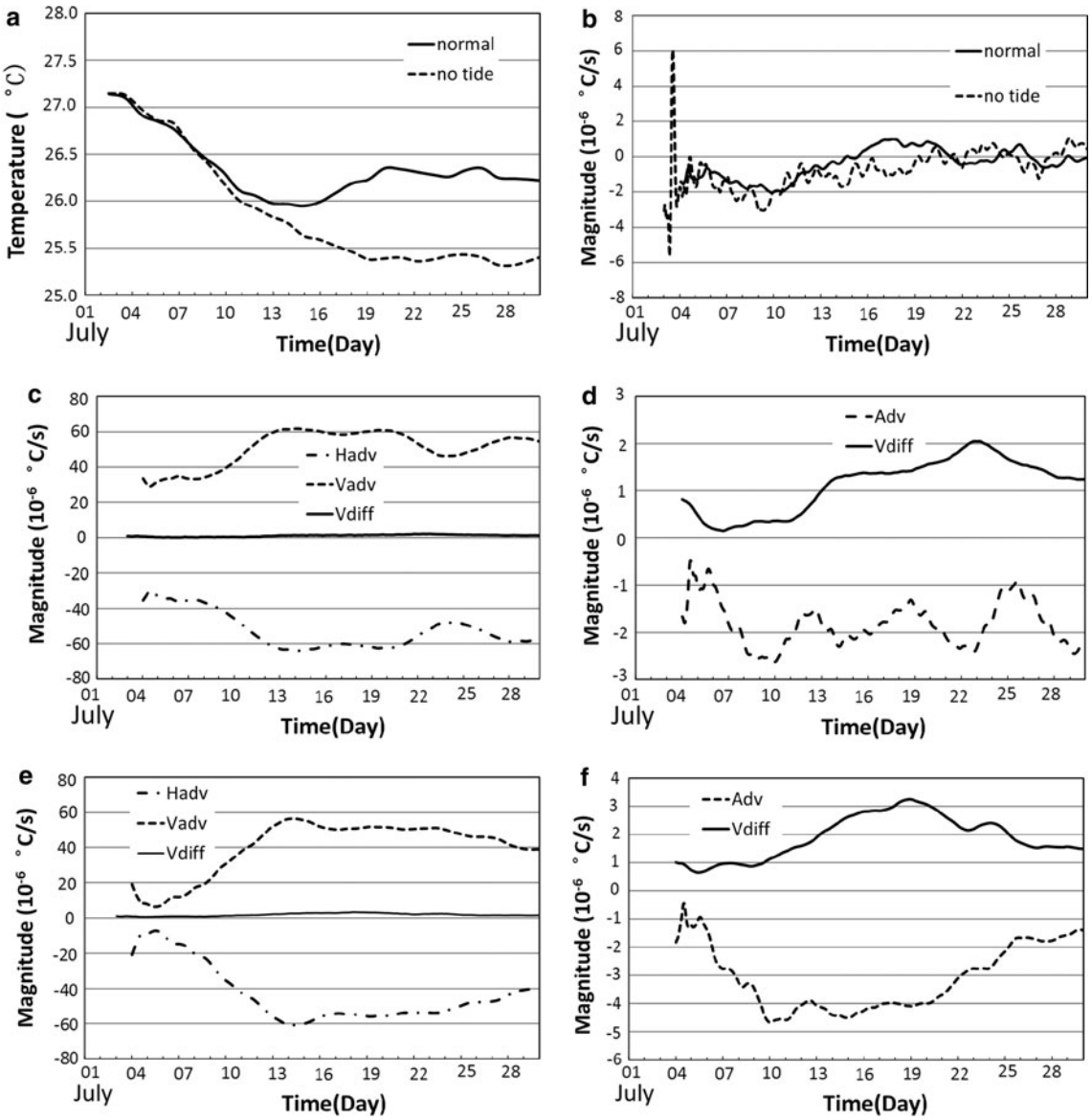

Fig. 8 Time series of filtered temperature (**a**) and filtered temperature changing rate (**b**), filtered terms in Eq. 1 from the model of normal case (**c**, **d**) and no tide case (**e**, **f**) at the surface layer in the Southwest upwelling region

tide; normal case) and without tidal forcing (no tide case) were run to generate the results presented in the following analysis.

To analyze the mechanism of the heat dynamics, the time variation of each term was calculated in the temperature conservation equation.

$$\overbrace{\frac{1}{D}\frac{\partial TD}{\partial t}}^{1}=\frac{1}{D}\left[\overbrace{-\frac{\partial TuD}{\partial x}-\frac{\partial TvD}{\partial y}}^{2}-\overbrace{\frac{\partial T\omega}{\partial \sigma}}^{3}+\overbrace{\frac{\partial}{\partial \sigma}\left(\frac{K_{\mathrm{H}}}{D}\frac{\partial T}{\partial \sigma}\right)}^{4}+F_{\mathrm{T}}-\frac{\partial R}{\partial z}\right] \quad (1)$$

where $D = H + \eta$ (H = bottom topography and η = surface elevation), ω is the vertical velocity in the σ coordinates, K_{H} the vertical diffusive coefficient, F_{T} the horizontal diffusion term, and $\frac{\partial R}{\partial z}$ the net heat flux at surface which is provided by the data from Mercator Ocean in our model of the TWS. The terms in Eq. 1 are temperature changing rate, *Trate* (term 1); horizontal advection, *Hadv* (term 2); vertical advection *Vadv* (term 3); vertical diffusion, *Vdiff* (term 4), and the F_{T} and $\frac{\partial R}{\partial z}$ which have smaller scales compared to the other terms. The inertial cycle boxcar filter is used to eliminate the tidal variations of each term in Fig. 8. The sum of *Hadv* and *Vadv* is referred to as total advection, *Adv*, for convenience in the analysis because *Hadv* and *Vadv* balance each other (see Fig. 8c, e).

Comparing Fig. 6c (no tide case) with Fig. 6b (normal case), one can see that the Southwest upwelling is less

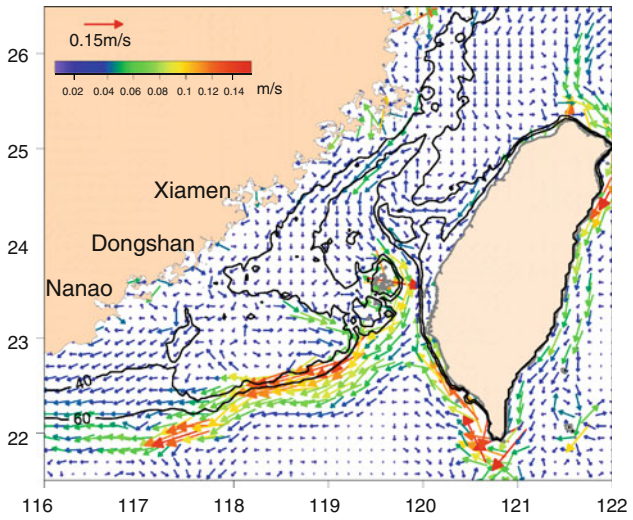

Fig. 9 Vertical averaged tidal residual current in the Taiwan Strait, with the 40 and 60 m depth contours plotted

pronounced when the tidal forcing is included in the model, i.e. less cold water on the coastal side of Section A. Figure 8a shows that the surface temperature in the Southwest upwelling is colder in the no tide case than that in the normal case from July 10, and the difference reaches a maximum of approximately 1°C on July 20. Corresponding to the temperature change, the *Trate* in Fig. 8b remains negative until July 20 in the no tide case while it has a higher value and switches to be positive on July 15 in the normal case. Figure 8f shows that *Adv* reaches a minimum from July 10 to 20 in the no tide case, but it keeps a higher value with tidal forcing (Fig. 8d), indicating that the tidal processes weaken the cross-isobath advection of the colder water from the coastal current upstream. When the sub-domain is driven by tidal elevation at lateral boundary only, the vertical mean tidal residual current (Fig. 9) can be derived from the tidal current harmonic analysis. It shows that the tidal processes maintain an off-shoreward residual current near the 40 and 60 m depth contours off Nanao with a magnitude of approximately 0.05 m s^{-1} in the opposite direction to the coastal current, that has a vertical mean magnitude of approximately 0.20 m s^{-1}, weakening the transport and advection of cold water from SCS to the Southwest upwelling region.

Comparing Fig. 5b with d, one can see that the cold water at the surface near the Taiwan Bank disappears when the tidal forcing is excluded from the model. And Fig. 6c also shows the warmer water occupies the water volume over the Taiwan Bank in the no tide case. As shown in Fig. 6f, the vertical diffusion coefficient southeast of the Taiwan Bank (i.e. at the distance of 130 km in Fig. 6) is 10^{-3} m^2 s^{-1} near the bottom and surface layers and $<10^{-5}$ $m^2 s^{-1}$ between 5 and 20 m in the no tide case. On the other hand, the inclusion of tidal forcing indicates that the vertical diffusion coefficient reaches 10^{-2} m^2 s^{-1} (Fig. 6e), implying that the tidal processes can increase the vertical mixing rate at the subsurface and thus diffuse the cold water to the surface by turbulence instead of by vertical velocity.

5 Summary

Using a nested circulation model based on the POM, we investigated the characteristics and mechanisms of two main upwellings (Southwest upwelling and Taiwan Bank upwelling) in the southern TWS. The cross-isobath current along the widened shelf, summer southwesterly monsoon and tidal processes are three main factors in generating the upwellings, but each factor plays a different role in the two upwelling regions.

Occurring in summer, the Southwest upwelling is induced by the local southwesterly monsoon wind and the upslope advection from southern deep water. For the Taiwan Bank upwelling, the ascending current exhibits a vertical velocity of approximately 1×10^{-4} m s^{-1} caused by the upward water transport from the lower layer, which is associated with the year-round northeastward-flowing SCS Warm Current near the southeast of the Taiwan Bank. This current carries the cold water from the SCS subsurface layer up to a depth of approximately 25 m near the edge of the Taiwan Bank.

The model sensitivity tests evaluate the contributions of wind and tide to these two upwellings. For the Southwest upwelling, the wind-driven Ekman transport can drive the cold water in the lower part of the water column to the surface, while the tidal processes generate an adverse tidal residual current of 0.05 m s^{-1} that weakens the coastal current and makes the cold water ascending from the head of widen shelf less pronounced. Regarding the Taiwan Bank upwelling, the strong tidal processes form the water volume with a high vertical mixing rate of about 10^{-2} m^2 s^{-1}, thoroughly mixing the water above the Taiwan Bank. The colder water at the southeast edge of the Taiwan Bank, being carried to the 25 m depth by the upward water transport from the lower layer, can hereafter be diffused up to the surface layer through strong tidal mixing, finally forming the Taiwan Bank upwelling.

Acknowledgments This work was supported by Grants 41076001 and 40810069004 from the Natural Science Foundation of China, Grant 2010121029 from the Fundamental Research Funds for the Central Universities, Grant from the Programme of Introducing Talents of Discipline to Universities (B07034), and Grant 2009CB421200 and 2010CB428904 from the National Basic Research Program of China. We thank the guest editor and three anonymous reviewers for helpful comments.

References

Arthur RS (1965) On calculation of vertical motion in eastern boundary currents from determinations of horizontal motion. J Geophys Res 70(12):2799–2803. doi:10.1029/JZ070i012p02799

Blanton JO, Atkinson LP, Pietrafesa LJ, Lee TN (1981) The intrusion of gulf-stream water across the continental-shelf due to topographically-induced upwelling. Deep Sea Res A 28(4):393–405. doi:10.1016/0198-0149(81)90006-6

Cai WJ, Lennon GW (1988) Upwelling in the Taiwan Strait in response to wind stress, ocean circulation and topography. Estuarine Coast Shelf Sci 26:15–31

Chen JQ (2011) Validation of QuikSCAT data and their application in the analysis of wind characteristics of Taiwan Strait and its adjacent waters in winter 2008. J Oceanogr Taiwan Strait 30(2):159–164 (in Chinese with English abstract)

Chen C, Beardsley RC, Limeburner R (1995) A numerical study of stratified tidal rectification over finite-amplitude banks. Part II: Georges Bank. J Phys Oceanogr 25(9):2111–2128

Fang GH, Kwok YK, Yu KJ, Zhu YH (1999) Numerical simulation of principal tidal constituents in the South China Sea, Gulf of Tonkin and Gulf of Thailand. Cont Shelf Res 19:845–869. doi:10.1016/S0278-4343(99)00002_3

Gan JP, Cheung A, Guo XG, Li L (2009) Intensified upwelling over a widened shelf in the northeastern South China Sea. J Geophys Res 114:C09019. doi:10.1029/2007JC004660

Garret C (2003) Internal tides and ocean mixing. Science 301(26):1858–1859. doi:10.1126/science.1090002

Garret C, Loucks RH (1976) Upwelling along the Yarmouth shore of Nova Scotia. J Fish Res Board Can 33(1):116–117

Guan BX, Chen SJ (1964) The current systems in the near-sea area of China Seas. Technical Report, Institute Of Oceanology, Chinese Academy of Sciences, Qingdao (in Chinese)

Hellerman S, Rosenstein M (1983) Normal monthly wind stress over the world ocean with error estimates. J Phys Oceanogr 13:1093–1104

Holloway PE, Barnes B (1998) A numerical investigation into the bottom boundary layer flow and vertical structure of internal waves on continental slope. Cont Shelf Res 18:31–65. doi:10.1016/S0278-4343(97)00067-8

Hong HS, Qiu SY, Ruan WQ, Hong GC (1991) Minnan-Taiwan bank fishing ground upwelling ecosystem study. In: Hong HS (ed) Minnan-Taiwan bank fishing ground upwelling ecosystem study. Science Press, Beijing, pp 1–18 (in Chinese with English abstract)

Hsu MK, Liu AK, Liu C (2000) A study of internal waves in the China Seas and Yellow Sea using SAR. Cont Shelf Res 20:389–410. doi:10.1016/S027-4343(99)00078-3

Hu JY, Liu MS (1992) The current structure during summer in southern Taiwan Strait. J Trop Oceanogr 11:42–47 (in Chinese with English abstract)

Hu JY, Kawamura H, Hong HS, Pan WR (2003) A review of research on the upwelling in the Taiwan Strait. Bull Mar Sci 73(3):605–628

Hu JY, Kawamura H, Li CY, Hong HS, Jiang YW (2010) Review on current and seawater volume transport through the Taiwan Strait. J Oceanogr 66(5):591–610. doi:10.1007/s10872-010-0049-1

Jan S, Wang J, Chern CS, Chao SY (2002) Seasonal variation of the circulation in the Taiwan Strait. J Mar Syst 35:249–268. doi:10.1016/S0924-7963(02)00130-6

Jan S, Chern CS, Wang J, Chao SY (2004) The anomalous amplification of M2 tide in the Taiwan Strait. Geophys Res Lett 31:L07308. doi:10.1029/2003GL019373

Jan S, Sheu DD, Kuo HM (2006) Water mass and through flow transport variability in the Taiwan Strait. J Geophys Res 111:C12012. doi:10.1029/2006JC003656

Janowitz GS, Pietrafesa LJ (1982) The effects of alongshore variation in bottom topography on a boundary current (topographically induced upwelling). Cont Shelf Res 1(2):123–141. doi:10.1016/0278-4343(82)90001-2

Jiang YW (2007) The now-cast system for the current of the Taiwan Strait, a study of three-dimensional numerical model. Technical Report, State Key Laboratory of Marine Environmental Science, Xiamen University, Xiamen, Fujian, China, p 135 (in Chinese)

Jing Z, Qi Y, Du Y (2011) Upwelling in the continental shelf of northern South China Sea associated with 1997–1998 El Niño. J Geophys Res 116(C2). doi:10.1029/2010jc006598

Li L, Li D (1989) Summer hydrographic features of channel west of Taiwan shoals and the coastal upwelling. J Oceanogr Taiwan Strait 8:353–359 (in Chinese with English abstract)

Lin FQ et al (1999) Analysis on temperature and salinity distributions in southern Taiwan Strait in August 1997. J Xiamen Univ 38:578–583 (in Chinese with English abstract)

Liu G, Chai F (2009) Seasonal and interannual variation of physical and biological processes during 1994–2001 in the Japan/East Sea; a three-dimensional physical–biogeochemical modeling study. J Mar Sci 78:265–277. doi:10.1016/j.jmarsys.2009.02.011

Loder JW, Wright DG (1985) Tidal rectification and frontal circulation on the sides of Georges Bank. J Mar Res 43:581–604

Matsumoto K, Takanezawa T, Ooe M (2000) Ocean tide models developed by assimilating TOPEX/POSEIDON altimeter data into hydrodynamical model: a global model and a regional model around Japan. J Oceanogr 56:567–581. doi:10.1023/A:1011157212596

Mellor GL (2004) Users guide for a three-dimensional, primitive equation, numerical ocean model. Program in atmospheric and oceanic sciences. Princeton University, NJ

Mellor GL, Oey LY, Ezer T (1998) Sigma coordinate pressure gradient errors and the seamount problem. J Atmos Ocean Technol 15(5):1122–1131

Oey LY, Chen P (1992) A nested-grid ocean model: with application to the simulation of meanders and eddies in the Norwegian coastal current. J Geophys Res 97:20063–20086. doi:10.1029/92JC01991

Pringle JM (2002) Enhancement of wind-driven upwelling and downwelling by alongshore bathymetric variability. J Phys Oceanogr 32(11):3101–3112. doi:10.1175/1520-0485(2002)

Qiao FL, Lu XG, Liu H, Ho CR, Liu CT (2008) Coastal upwelling in the South China Sea. In: Liu AK, Ho CR, Liu CT (eds) Satellite remote sensing of South China Sea. Tingmao, Taipei, pp 135–158

Tang DL, Kester DR, Ni IH, Kawamura H, Hong HS (2002) Upwelling in the Taiwan Strait during the summer monsoon detected by satellite and shipboard measurements. Remote Sens Environ 83:457–471. doi:10.1016/S0034-4257(02)00062-7

Tee KT, Smith PC, Lefaivre D (1993) Topographic upwelling off southwest nova-scotia. J Phys Oceanogr 23(8):1703–1726. doi:10.1175/1520-0485(1993)

Wang X, Chao Y (2004) Simulated sea surface salinity variability in the tropical Pacific. Geophys Res Lett 31:L02302. doi:10.1029/2003GL018146

Wu LX, Lin HY (1990) Preliminary analysis on summer upwelling near the continental shelf of eastern Guangdong. Trop Oceanol 9:16–23 (in Chinese with English abstract)

Xue HJ, Chai F, Pettigrew NRP (2000) A model study of the seasonal circulation in the Gulf of Maine. J Phys Oceanogr 30(5):1111–1135

Zhang C, Hu C, Shang S, Muller-Karger FE, Li Y, Dai M, Huang B, Ning X, Hong H (2006) Bridging between SeaWiFS and MODIS for continuity of chlorophyll-*a* concentration assessments off southeastern China. Remote Sensing Environ 102:250–263. doi:10.1016/j.rse.2006.02.015

Zimmerman JTF (1978) Topographic generation of residual circulation by oscillatory tidal currents. Geophys Astrophys Fluid Dyn 11:35–47